Tokyo Climate Center, Japan Meteorological Agency

TCC News

Autumn 2025

Table of Contents: TCC News No. 82

JMA's Seasonal Numerical Ensemble Prediction for Boreal Winter 2025/2026

This report outlines JMA's dynamical seasonal ensemble prediction for boreal winter 2025/2026 (December – February, referred to as DJF), which was used as a basis for JMA's operational cold season outlook issued on 21 October 2025. The outlook is based on JMA's seasonal ensemble prediction system (JMA/MRI-CPS3).

Summary: Based on JMA/MRI-CPS3, the La Niña-like conditions that emerged this autumn are likely to continue toward the first half of boreal winter with rapid weakening. The negative IOD-like sea surface temperature anomalies that also emerged this autumn are expected to remain in early winter. In association, active convection is expected from the eastern Indian Ocean to areas near the Maritime Continent. Conversely, inactive convection is expected over the western Indian Ocean and the equatorial Pacific near the dateline. This triple convection anomaly pattern is expected to force atmospheric circulation anomalies in the Asia-Pacific region.

1. Sea surface temperature

In September, volumes of cold subsurface water persisted in the central and eastern equatorial Pacific. JMA/MRI-CPS3 predicts a NINO.3 SST decrease due to the persistence of stronger-than-normal easterly winds over the equatorial Pacific toward the first half of boreal winter. However, La Niña-like conditions are not expected to persist due to expected atmosphere-ocean coupling, and the NINO.3 SST is expected to come closer to normal during late boreal winter. In conclusion, La Niña-like conditions are likely to continue toward the first half of boreal winter and rapidly weaken in the second half, making it likely (80%) that ENSO-neutral conditions will persist until late boreal winter. In the tropical Indian Ocean, the negative IOD-like sea surface temperature anomalies that emerged this autumn are expected to remain in early winter. Reflecting these ENSO- and IOD-related conditions, negative anomalies are expected from the eastern to central equatorial Pacific and in the western tropical Indian Ocean, while positive anomalies are expected in the western tropical Pacific and the eastern tropical Indian Ocean in DJF (Figure

1-1).

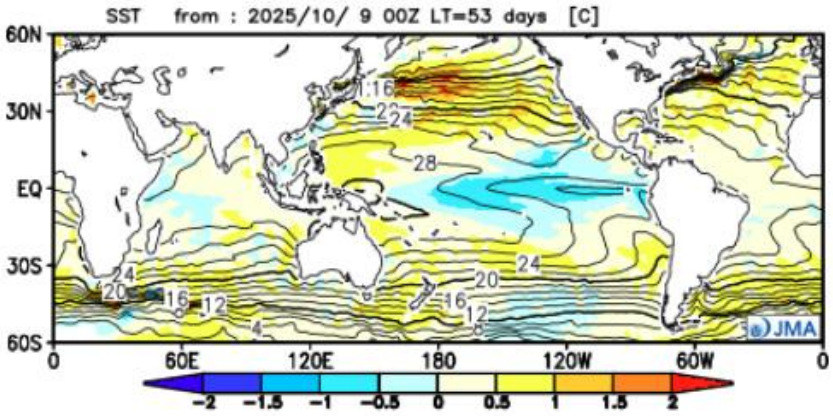

Figure 1-1 Predicted SSTs (contours) and SST anomalies (shading) for December 2025–February 2026 (ensemble mean of 51 members)

2. Prediction for the tropics and sub-tropics

Figure 1-2 (a) shows predicted precipitation (contours) and related anomalies (shading) for DJF. In association with SST anomalies over the tropics, precipitation is expected to be above normal from the eastern Indian Ocean to the Maritime Continent and below normal over the western Indian Ocean and the central Pacific.

Figure 1-2 (b) shows predicted velocity potential (contours) and related anomalies (shading) in the upper troposphere for DJF. In association with the precipitation anomalies described above, negative (i.e., large-scale divergent) anomalies are expected from the eastern Indian Ocean to the Maritime Continent, while positive (large-scale convergence) anomalies are expected over the western Indian Ocean and the western and central Pacific.

Figure 1-2 (c) shows predicted stream functions (contours) and related anomalies (shading) in the upper troposphere for DJF. Cyclonic and anti-cyclonic circulation anomalies (i.e., negative and positive in the Northern Hemisphere, respectively) are expected over the northwestern Indian Ocean and the southeastern Eurasian continent, respectively, while weak cyclonic circulation anomalies are predicted near Japan. The resulting wavy patten is a manifestation of a stationary Rossby wave packet forced by tropical convection anomalies and propagating along the subtropical jet stream (STJ), inducing related meandering.

Figure 1-2 (d) shows predicted stream functions (contours) and related anomalies (shading) in the lower troposphere for DJF. Anti-cyclonic and cyclonic circulation anomalies straddling the equator are expected over the Pacific and from the Indian Ocean to the Maritime Continent, respectively, due to forcing by tropical convection anomalies.

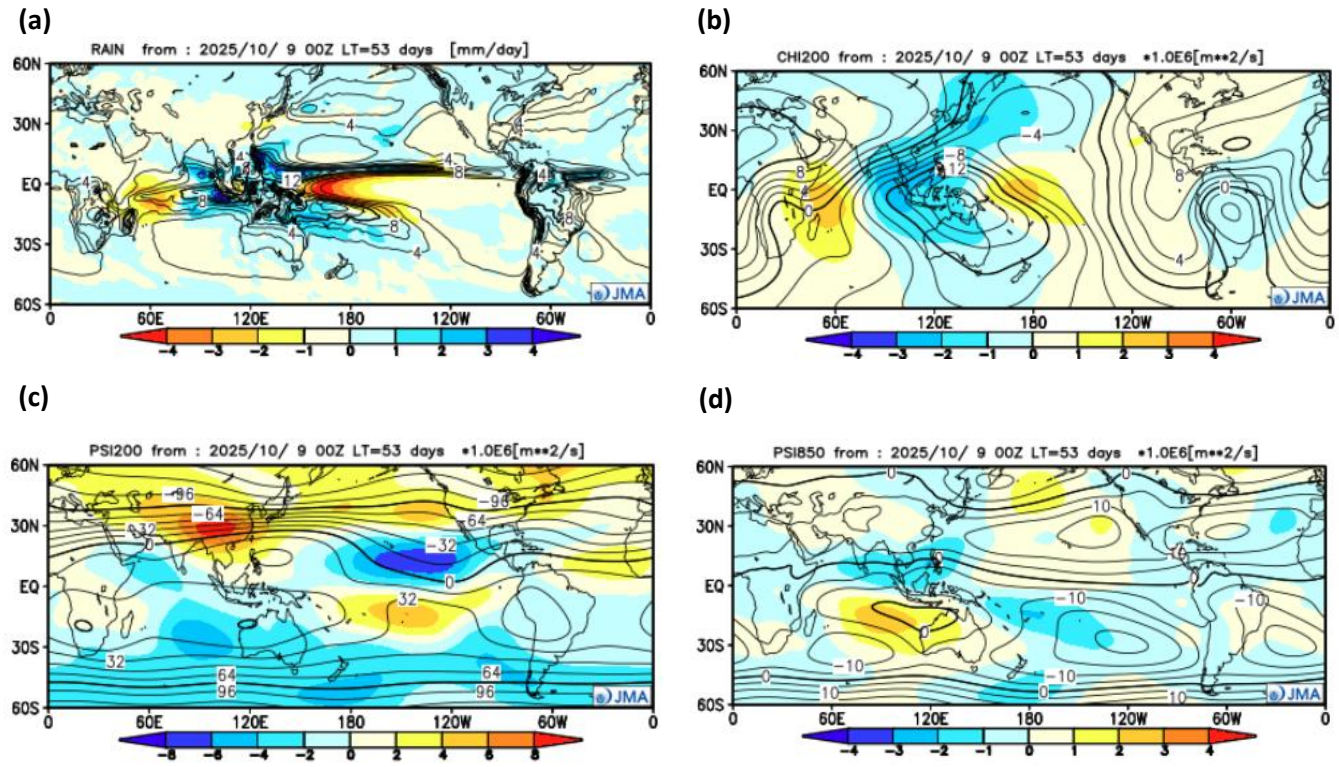

Figure 1-2 Predicted atmospheric fields over 60°N-60°S for December 2025 – February 2026 (ensemble mean of 51 members)

(a) Precipitation (contours) and anomaly (shading). The contour interval is 2 mm/day. (b) Velocity potential at 200-hPa (contours) and anomaly (shading). The contour interval is 2×10^6 m^2/s. (c) Stream function at 200-hPa (contours) and anomaly (shading). The contour interval is 16×10^6 m^2/s. (d) Stream function at 850-hPa (contours) and anomaly (shading). The contour interval is 5×10^6 m^2/s.

3. Prediction for the mid- and high- latitudes of the Northern Hemisphere

Figure 1-3 (a) shows predicted 500-hPa geopotential heights (contours) and related anomalies (shading) for DJF. Positive anomalies are predicted over a wide area of the Northern Hemisphere with significantly positive anomalies over the central Pacific in the mid-latitudes and from the eastern part of North America to the Arctic region. Weak negative anomalies are predicted over Japan in association with southward STJ meandering.

Figure 1-3 (b) shows predicted sea level pressure (contours) and related anomalies (shading) for DJF. The Icelandic Low is predicted to be weaker than normal, and the Aleutian Low is predicted to be stronger/weaker than normal in western and central parts, respectively.

(a) (b)

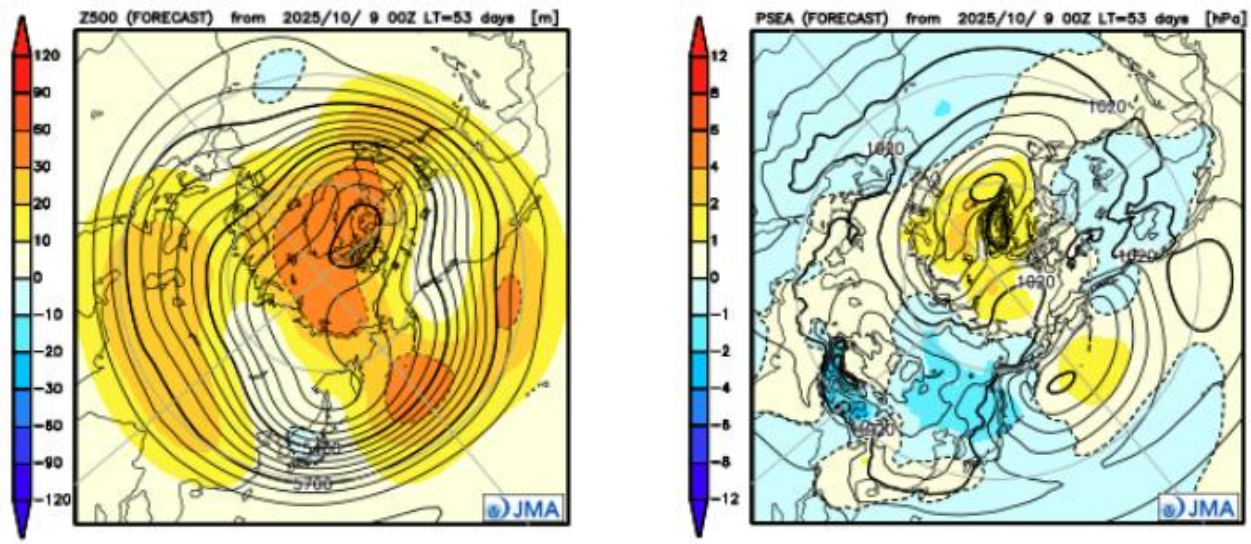

Figure 1-3 Predicted atmospheric fields over the Northern Hemisphere for December 2025 – February 2026 (ensemble mean of 51 members)

(a) Geopotential height at 500-hPa (contours) and anomaly (shading). The contour interval is 60 m. (b) Sea level pressure (contours) and anomaly (shading). The contour interval is 4 hPa.

Note: JMA operates a seasonal Ensemble Prediction System (EPS) using the Coupled atmosphere-ocean General Circulation Model (CGCM) to make seasonal predictions beyond a one-month time range. The EPS produces perturbed initial conditions by means of a combination of the initial perturbation method and the lagged average forecasting (LAF) method. Prediction is made using 51 members from the latest 17 initial dates (3 members are used every day). Details of the prediction system and verification maps based on 30-year hindcast experiments (1991–2020) are available at https://ds.data.jma.go.jp/tcc/tcc/products/model/.

(MAEDA Shuhei, Tokyo Climate Center)

<<Table of contents <Top of this article

Summary of the 2025 Asian Summer Monsoon

This report summarizes the characteristics of the surface climate and atmospheric/oceanographic conditions related to the Asian summer monsoon for 2025.

Note: The Japanese Reanalysis for Three Quarters of a Century (JRA-3Q) dataset (Kosaka et al. 2024) and MGDSST (Kurihara et al. 2006) were used to analyze atmospheric circulation and sea surface temperature (SST) in the research reported here. NOAA Climate Prediction Center (CPC) blended Outgoing Longwave Radiation (OLR) data from the NOAA website (https://ftp.cpc.ncep.noaa.gov/precip/CBO_V1/) were used to infer tropical convective activity. The base period for the normal is 1991 to 2020. The term “anomaly” as used in this report refers to deviation from the normal.

1. Precipitation and temperature

CLIMAT data on total precipitation for the summer monsoon season (June – September) showed more than 140% of the normal in and around northern India, southern Pakistan and the eastern Indochina Peninsula, over parts of northeastern China and eastern Mongolia, and from southern Indonesia to western Papua New Guinea. Elsewhere, less than 60% of the normal was seen over the eastern Middle East, in and around Sri Lanka and over western Mongolia (Figure 2-1 (a)). Notable values exceeding 180% of the normal were seen around northern India and southern Pakistan, and it was reported that heavy rains from June to August caused at least 1,380 fatalities in Nepal, India and Pakistan (sources: European Commission, EM-DAT, governments of Nepal and Pakistan). It was also reported that heavy rains from June to August and Typhoons Wipha, Francisco and Co-may in July caused at least 190 fatalities in China (sources: EM-DAT) and at least 80 in China, the Philippines, Vietnam and Myanmar (sources: European Commission, EM-DAT). In September, it was reported that heavy rains and Typhoons Ragasa and Bualoi caused at least 200 fatalities in Nepal, India and Pakistan (sources: European Commission, EM-DAT, governments of Nepal and Pakistan) and at least 170 from southeastern China to northern Southeast Asia (sources: EM-DAT).

Four-month mean temperatures for the same period were above normal over a wide area of mid-latitude Eurasia, particularly from around Pakistan to western China and from eastern China to around Japan, while values were below normal in parts of India and the Indochina Peninsula (Figure 2-1 (b)). In Japan and the Republic of Korea, summer (June to August) mean temperatures were at record highs since 1898 and 1973, respectively (sources: Japan Meteorological Agency, Korea Meteorological Administration).

(a) (b)

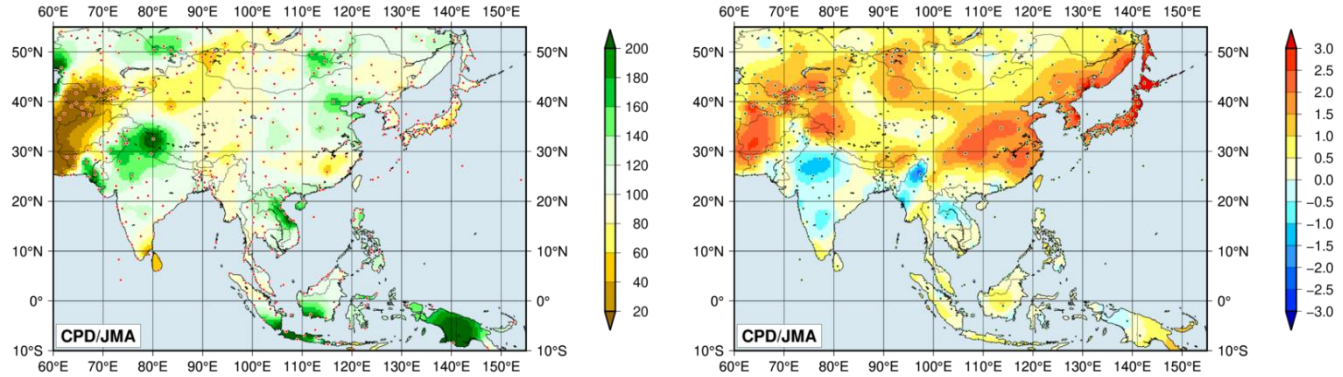

Figure 2-1 Four-month (a) precipitation ratios [%] and (b) mean temperature anomalies [°C] from June to September 2025

The base period for normal is 1991 – 2020. The red (a) and green (b) dots show stations providing map data, which are interpolated due to a lack of CLIMAT reporting and climatological normal values in some areas.

2. Tropical cyclones

A total of 20 named tropical cyclones (TCs) had formed over the western North Pacific and the South China Sea by the end of September 2025, compared with the normal of 18.6 (Table 2-1). June to September saw a total of 20 named TCs (climatological normal: 16.1), with 19 approaches or landfalls on Southeast and East Asia and 11 (climatological normal: 9.5) on Japan. No TCs had formed by May (climatological normal: 2.5) under suppressed convection in the tropical western North Pacific. However, the total number of named TCs had increased to 20 by the end of September, likely due to enhanced convection from the South China Sea to the tropical western North Pacific, in association with enhanced Asian monsoonal convection and frequent intrusions of upper-level high potential vorticity (PV) air masses over warmer ocean waters (Section 3).

Table 2-1 Named tropical cyclones over the western North Pacific and the South China Sea by the end of September 2025

Name (number)		Date(UTC)	Category[1)]	Maximum wind[2)] (kt)
Wutip	(2501)	11 Jun - 14 Jun	STS	55
Sepat	(2502)	23 Jun - 24 Jun	TS	35
Mun	(2503)	2 Jul - 7 Jul	STS	50
Danas	(2504)	4 Jul - 8 Jul	TY	75
Nari	(2505)	12 Jul - 14 Jul	TS	45
Wipha	(2506)	18 Jul - 22 Jul	STS	60
Francisco	(2507)	23 Jul - 25 Jul	TS	40
Co-may	(2508)	23 Jul - 30 Jul	STS	60
Krosa	(2509)	24 Jul - 4 Aug	TY	75
Bailu	(2510)	3 Aug - 5 Aug	TS	35
Podul	(2511)	7 Aug - 14 Aug	TY	80
Lingling	(2512)	21 Aug	TS	40
Kajiki	(2513)	23 Aug - 26 Aug	TY	80
Nongfa	(2514)	30 Aug	TS	40
Peipah	(2515)	3 Sep - 5 Sep	TS	45
Tapah	(2516)	6 Sep - 8 Sep	TY	65
Mitag	(2517)	18 Sep - 19 Sep	TS	45
Ragasa	(2518)	18 Sep - 25 Sep	TY	110
Neoguri	(2519)	18 Sep - 28 Sep	TY	105
Bualoi	(2520)	23 Sep - 29 Sep	TY	75

Note: Based on information from the RSMC Tokyo-Typhoon Center. Tropical cyclones from Bailu (2510) to Bualoi (2520) are based on early analysis data (rather than best track data).

1) Intensity classification for tropical cyclones.
TS: tropical storm (34 – 47 kt), STS: severe tropical storm (48 – 63 kt), TY: typhoon (≥64 kt)

2) Estimated maximum 10-minute mean wind.

3. Monsoon activity and atmospheric circulation

Convective activity inferred from OLR averaged for June – September 2025 (Figure 2-2) was enhanced around the Maritime Continent, over northwestern India, and from the Bay of Bengal to the east of the Philippines, and was suppressed over the western Indian Ocean and the western equatorial Pacific. The anomalous convection observed from the Indian Ocean to the western North Pacific around the equator was associated with SSTs featuring positive anomalies around the Maritime Continent and negative anomalies over the western Indian Ocean and central to eastern parts of the equatorial Pacific (Figure 2-3). OLR index values (Table 2-2) indicate that the overall activity of the Asian summer monsoon (represented by the SAMOI (A) index) was above normal, particularly in June and September. The active convection area was significantly shifted northeastward from its normal position in July (see the SAMOI (N) and SAMOI (W) indices), but was shifted northwestward in May accompanied by early onset of the Indian monsoon (Indian Meteorological Department 2025).

Convective activity in the Asian monsoon region exhibited intra-seasonal variations. Convection over India and the Bay of Bengal was generally enhanced except in early June and from the end of July to the beginning of August (Figure 2-4 (a)). Convection over the Philippines was also generally enhanced except from the end of July to the beginning of August, with significant enhancement in mid-July (Figure 2-4 (b)). The markedly enhanced convection observed was probably related to unprecedented intensification of boreal summer intra-seasonal oscillation (BSISO; Lee et al. 2013; Kikuchi 2021) accompanied by a series of TC occurrences in July (Table 2-1), and was followed by an intensified Pacific-Japan (PJ) pattern (Nitta 1987; Kosaka and Nakamura 2006).

Figure 2-5 shows four-month mean 200- and 850-hPa stream function fields for June – September 2025. In the upper troposphere (Figure 2-5 (a)), anti-cyclonic circulation anomalies straddling the equator were seen around the Indian Ocean in association with enhanced convection around the Maritime Continent and from the Bay of Bengal to the east of the Philippines. The Tibetan High extended northward and northeastward, resulting in above-normal temperatures over a wide area of mid-latitude Eurasia (Section 1). The anomalous extension of the Tibetan High was attributable to enhanced Asian monsoonal convection (Figure 2-2), and the Silk-Road pattern (Enomoto 2003) manifested as a wavy anomaly pattern along the subtropical jet stream over Eurasia. Upper-level anti-cyclonic and cyclonic circulation anomalies were seen to the east and southeast of Japan, respectively, in association with frequent appearance of Rossby-wave breaking. Upper-level high-PV air masses consequently detached from the mid-Pacific trough (Figure 2-6) and migrated toward the southeast of Japan, contributing to enhanced convection and possibly a series of TC generations from July onwards through dynamically induced ascent (Takemura et al. 2017).

In the lower troposphere (Figure 2-5 (b)), cyclonic circulation anomalies straddling the equator were seen from the Indian Ocean to the Maritime Continent, and anti-cyclonic circulation anomalies straddling the equator were seen over the western tropical Pacific. The North Pacific Subtropical High (NPSH) was stronger than normal and extended toward Japan, contributing to significantly above-normal temperatures around eastern East Asia. The extended NPSH is attributable to enhanced convection around the Philippines (Figure 2-2), as per the intensified PJ pattern.

The above-normal temperatures observed over a wide area of mid-latitude Eurasia (Figure 2-1 (b)) corresponded to the significant northward shift of the subtropical jet and associated above-normal temperatures over the mid-latitudes of the Northern Hemisphere (Figures 2-7a and b), possibly in association with significantly above-normal SSTs in the mid-latitude North Pacific (Figure 2-3). In addition, the above-normal temperatures observed throughout the troposphere (Figure 2-7b) may be attributable to the long-term rising trend of air temperature.

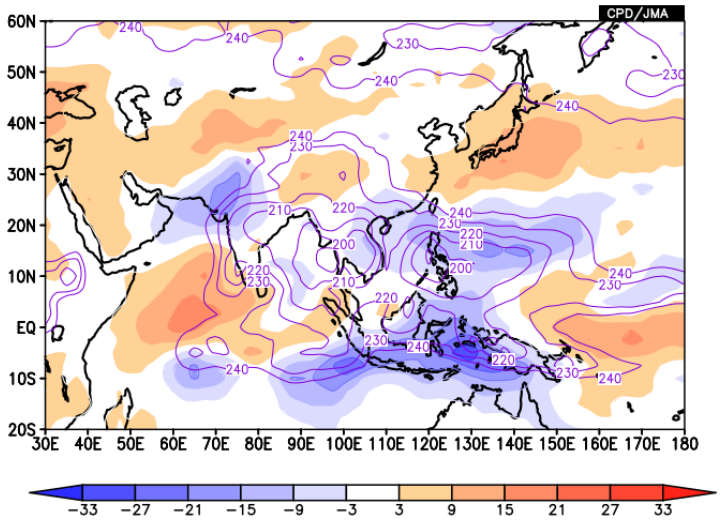

Figure 2-2 Four-month mean OLR [W/m^2] for June–September 2025

Contours indicate OLR lower than 240 W/m^2 at intervals of 10 W/m^2, and color shading denotes OLR anomalies from the normal (i.e., the 1991–2020 average). Negative (cold color) and positive (warm color) OLR anomalies show enhanced and suppressed convection compared to the normal, respectively.

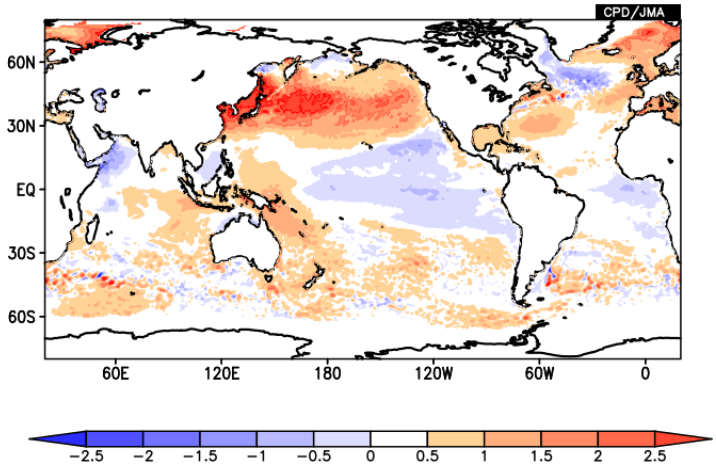

Figure 2-3 Four-month mean SST anomalies [°C] for June–September 2025

The base period for the normal is 1991 – 2020.

Table 2-2 Summer Asian Monsoon OLR Index (SAMOI) values observed from May to September 2025

Asian summer monsoon OLR indices (SAMOI) are derived from OLR anomalies. SAMOI (A), (N) and (W) indicate the overall activity of the Asian summer monsoon, its northward shift and its westward shift, respectively. SAMOI definitions are as follows: SAMOI (A) = (-1) × (W + E); SAMOI (N) = S – N; SAMOI (W) = E – W. W, E, N and S indicate area-averaged OLR anomalies for the respective regions shown in the figure on the right normalized by their standard deviations.

	Summer Asian Monsoon OLR Index (SAMOI)		
	SAMOI (A): Activity	SAMOI (N): Northward-shift	SAMOI (W): Westward-shift
May 2025	+0.9	+0.7	+1.7
Jun 2025	+1.2	+0.4	-0.8
Jul 2025	+0.5	+2.0	-1.6
Aug 2025	+0.1	-0.8	-1.0
Sep 2025	+1.1	+0.9	+0.4

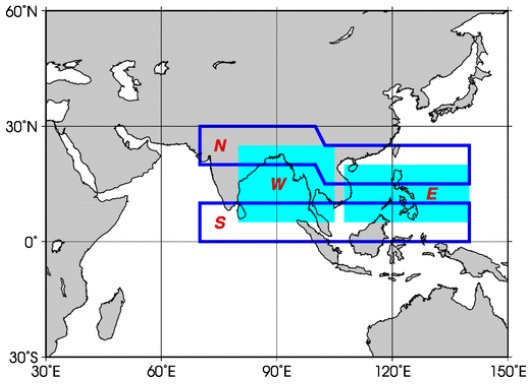

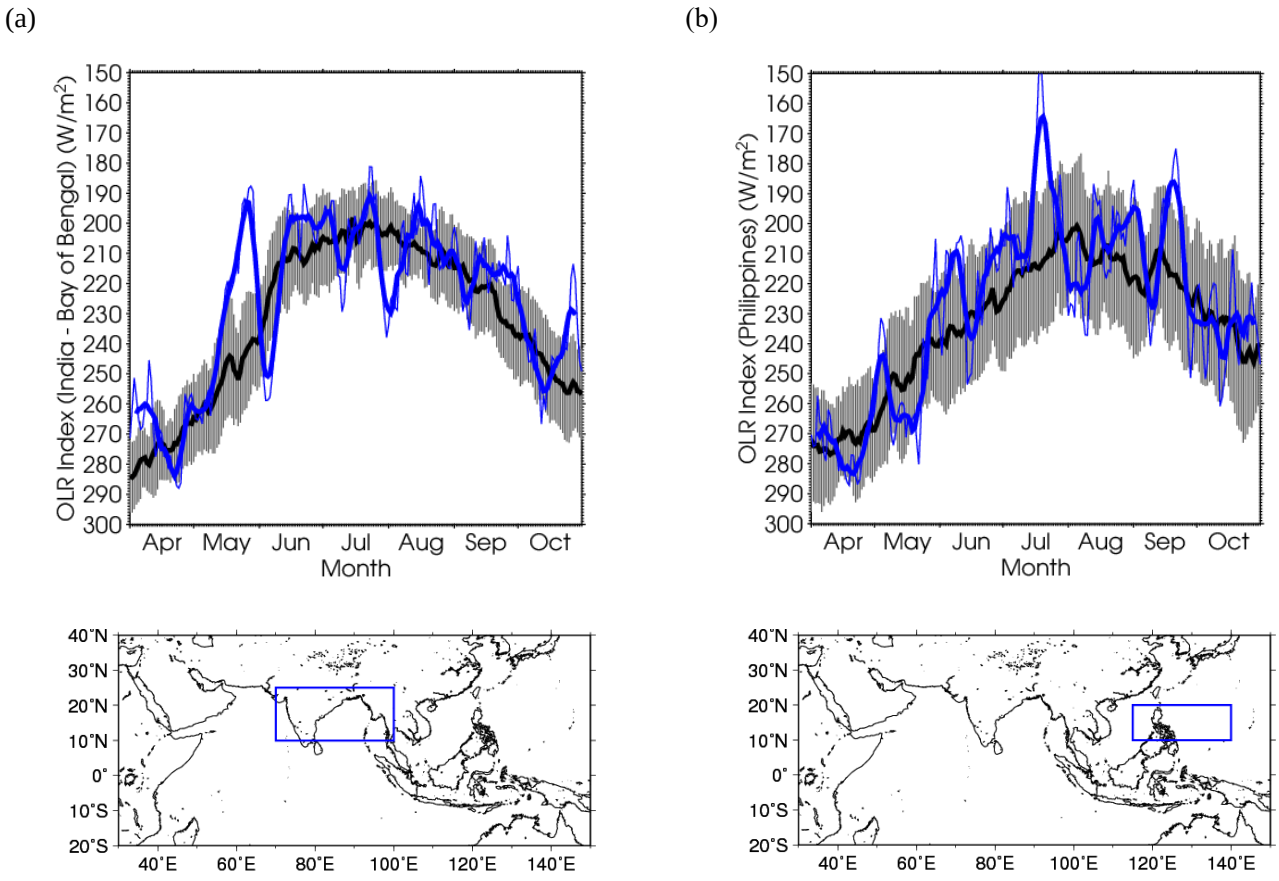

Figure 2-4 Time-series representation of OLR [W/m²] averaged over (a) India and the Bay of Bengal (shown by the rectangle on the bottom: 10°N - 25°N, 70°E - 100°E) and (b) the Philippines (shown by the rectangle on the bottom: 10°N - 20°N, 115°E - 140°E) during a period from April to October 2025

The OLR indices are calculated after Wang and Fan (1999). The thick and thin blue lines indicate seven-day running mean and daily mean values, respectively. The black line denotes the normal (i.e., the 1991 - 2020 average), and the gray shading shows the range of the standard deviation calculated for the time period of the normal.

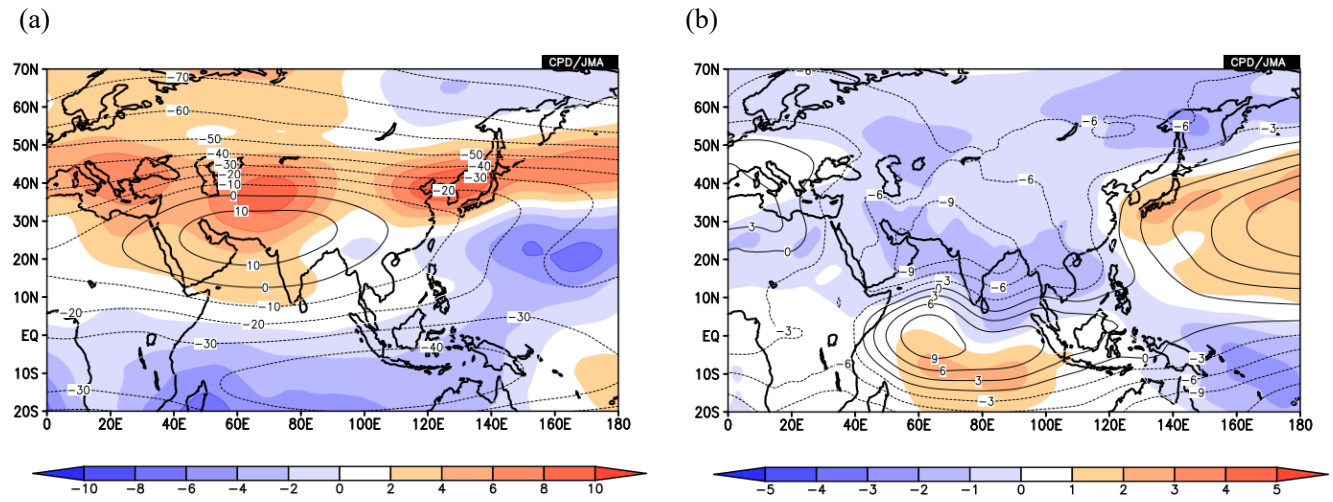

Figure 2-5 Four-month mean (a) 200-hPa and (b) 850-hPa stream function [10^6 m²/s] for June–September 2025

Contours indicate stream function at intervals of (a) 10 × 10^6 m²/s and (b) 3 × 10^6 m²/s, and shading shows stream function anomalies. Red (blue) shading denotes anti-cyclonic (cyclonic) circulation anomalies in the Northern Hemisphere, and vice-versa in the Southern Hemisphere. The base period for the normal is 1991 – 2020.

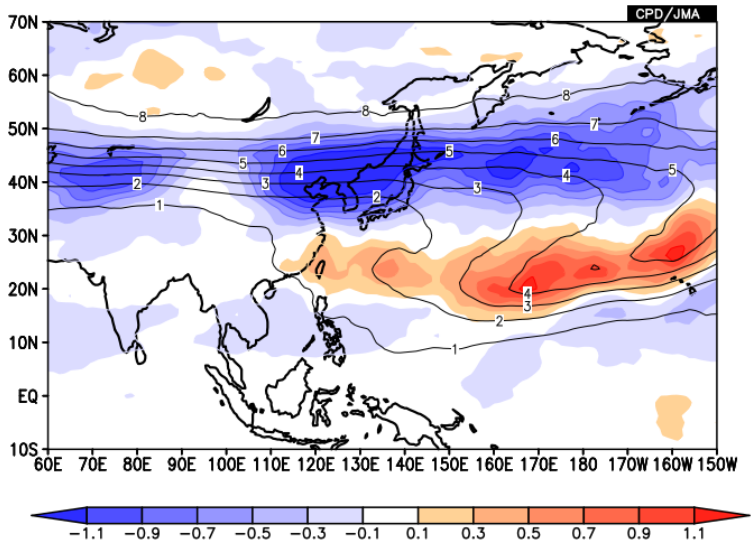

Figure 2-6 Four-month mean 360-K isentropic potential vorticity [PVU; $10^{-6}m^2s^{-1}K\ kg^{-1}$] for June–September 2025

Shading indicates anomalies, and contours show potential vorticity at intervals of 1 PVU. The base period for the normal is 1991 – 2020.

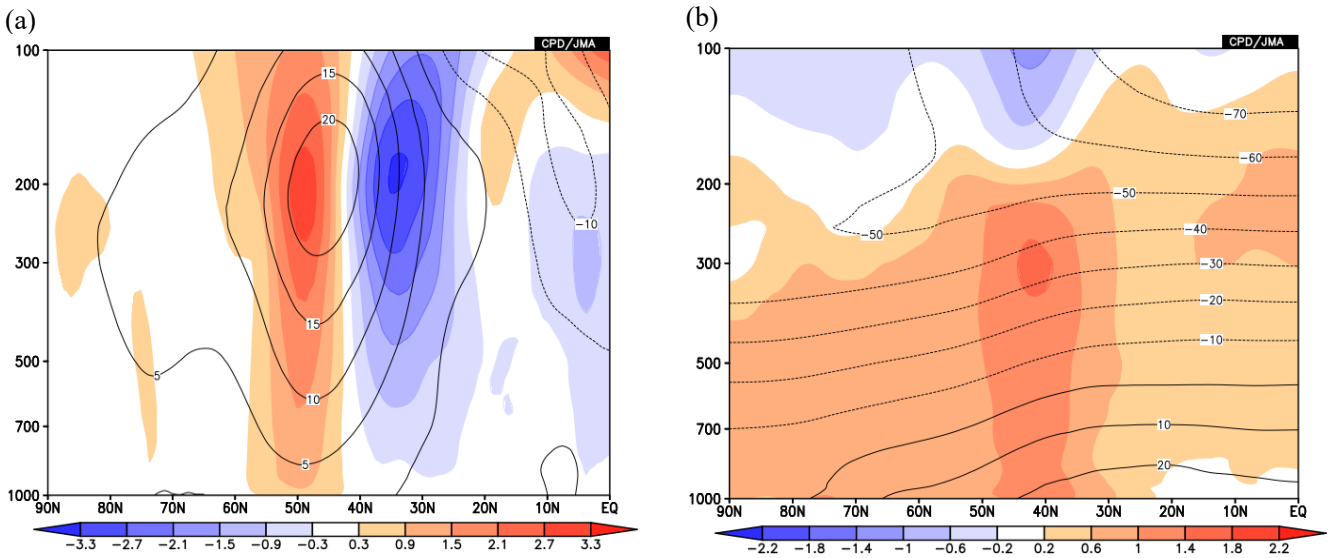

Figure 2-7 Latitude-pressure [hPa] section of zonally-averaged (a) zonal wind [m/s] and (b) temperature [°C] in the Northern Hemisphere for June-September 2025

Shading indicates anomalies, and contours show zonal wind at intervals of (a) 5m/s and (b) 10°C. The base period for the normal is 1991 – 2020.

References

Enomoto, T., B. J. Hoskins, and Y. Matsuda, 2003: The formation mechanism of the Bonin high in August. *Quart. J. Roy. Meteor. Soc.*, **129**, 157–178. https://doi.org/10.1256/qj.01.211

Indian Meteorological Department, 2025: Advance of southwest monsoon 2025. (available at https://mausam.imd.gov.in/imd_latest/contents/monsoon.php, accessed in 30 September 2025)

Kikuchi, K., 2021: The boreal summer intraseasonal oscillation (BSISO): A review. *J. Meteor. Soc. Japan*, **99**, 933-972. https://doi.org/10.2151/jmsj.2021-045

Kosaka, Y., and H. Nakamura, 2006: Structure and dynamics of the summertime Pacific-Japan teleconnection pattern. *Quart. J. Roy. Meteor. Soc.*, **132**, 2009-2030. https://doi.org/10.1256/qj.05.204

Kosaka Y., S. Kobayashi, Y. Harada, C. Kobayashi, H. Naoe, K. Yoshimoto, M. Harada, N. Goto, J. Chiba, K. Miyaoka, R. Sekiguchi, M. Deushi, H. Kamahori, T. Nakaegawa; T. Y. Tanaka, T. Tokuhiro, Y. Sato, Y. Matsushita, and K. Onogi, 2024: The JRA-3Q Reanalysis. *J. Meteor. Soc. Japan*, **102**, 49-149. https://doi.org/10.2151/jmsj.2024-004

Kurihara, Y., T. Sakurai, and T. Kuragano, 2006: Global daily sea surface temperature analysis using data from satellite microwave radiometer, satellite infrared radiometer and in-situ observations. *Weather Service Bulletin*, **73**, Special issue, s1-s18 (in Japanese).

Lee, J.-Y., B. Wang, M. C. Wheeler, X. Fu, D. E. Waliser, and I.-S. Kang, 2013: Real-time multivariate indices for the boreal summer intraseasonal oscillation over the Asian summer monsoon region. *Clim. Dyn.*, **40**, 493-509. https://doi.org/10.1007/s00382-012-1544-4

Nitta, T., 1987: Convective activities in the tropical western Pacific and their impact on the Northern Hemisphere summer circulation. *J. Meteor. Soc. Japan*, **65**, 373-390. https://doi.org/10.2151/jmsj1965.65.3_373

Takemura, K., Y. Kubo, and S. Maeda, 2017: Relation between a Rossby wave-breaking event and enhanced convective activities in August 2016. *SOLA*, **13**, 120-124. https://doi.org/10.2151/sola.2017-022

Wang, B., and Z. Fan, 1999: Choice of South Asian summer monsoon indices. *Bull. Amer. Meteor. Soc.*, **80**, 629–638. https://doi.org/10.1175/1520-0477(1999)080<0629:COSASM>2.0.CO;2

(TAKEMURA Kazuto, YAMADA Ken, Tokyo Climate Center)

<<Table of contents <Top of this article

Status of the Antarctic Ozone Hole in 2025

The Antarctic ozone hole in 2025 expanded earlier than average for the most recent 10-year period due to a large low-temperature region in the stratosphere above Antarctica, but its annual maximum size was approximately equal to the average.

Since the early 1980s, the Antarctic stratospheric ozone level has fallen every year in austral spring with a peak in September or early October. This area of depletion is referred to as the Antarctic ozone hole.

Based on JMA analysis using data from the Ozone Mapper Profiler Suite (OMPS) on board the Suomi National Polar-orbiting Partnership (NPP) satellite, the Antarctic ozone hole in 2025 appeared in late July and expanded earlier than the most recent 10-year average, but was smaller than the average after mid-September (Figure 3-1, upper left). Its annual maximum size (observed on 9 September) was 22.8 million square kilometers, equivalent to approximately 1.6 times the size of Antarctica (Figure 3-1, upper right). This was close to the average of the most recent decade and also close to the 2024 value.

In July and August 2025, the polar vortex over Antarctica was stable, and the extent of the low-temperature region in the stratosphere was greater than the most recent 10-year average. As a result, formation of polar stratospheric clouds (PSCs), which play an important role in ozone depletion, was enhanced, leading to an earlier expansion of the ozone hole. After September, the low-temperature region was smaller than the most recent decadal average, and the ozone hole area also remained below average.

As an overall trend, the annual maximum size of the Antarctic ozone hole is very likely to have decreased since 2000 (statistically significant at a confidence level of 90%).The *WMO/UNEP Scientific Assessment of Ozone Depletion:*

2022 reports that total column ozone in the Antarctic continues to recover, notwithstanding substantial interannual variability in the size, strength and longevity of the ozone hole, and is expected to return to 1980 values around 2066.

The ozone layer acts as a shield against ultraviolet radiation, which can cause skin cancer. The Antarctic ozone hole was first recognized in the early 1980s, and large-scale events have been observed since the 1990s. Its maximum area on record was 29.8 million square kilometers (2000). Antarctic ozone depletion caused an expansion of the tropics and a poleward shift of the jet stream and storm tracks in the Southern Hemisphere that led to pronounced changes in summertime surface climate conditions according to recent assessment.

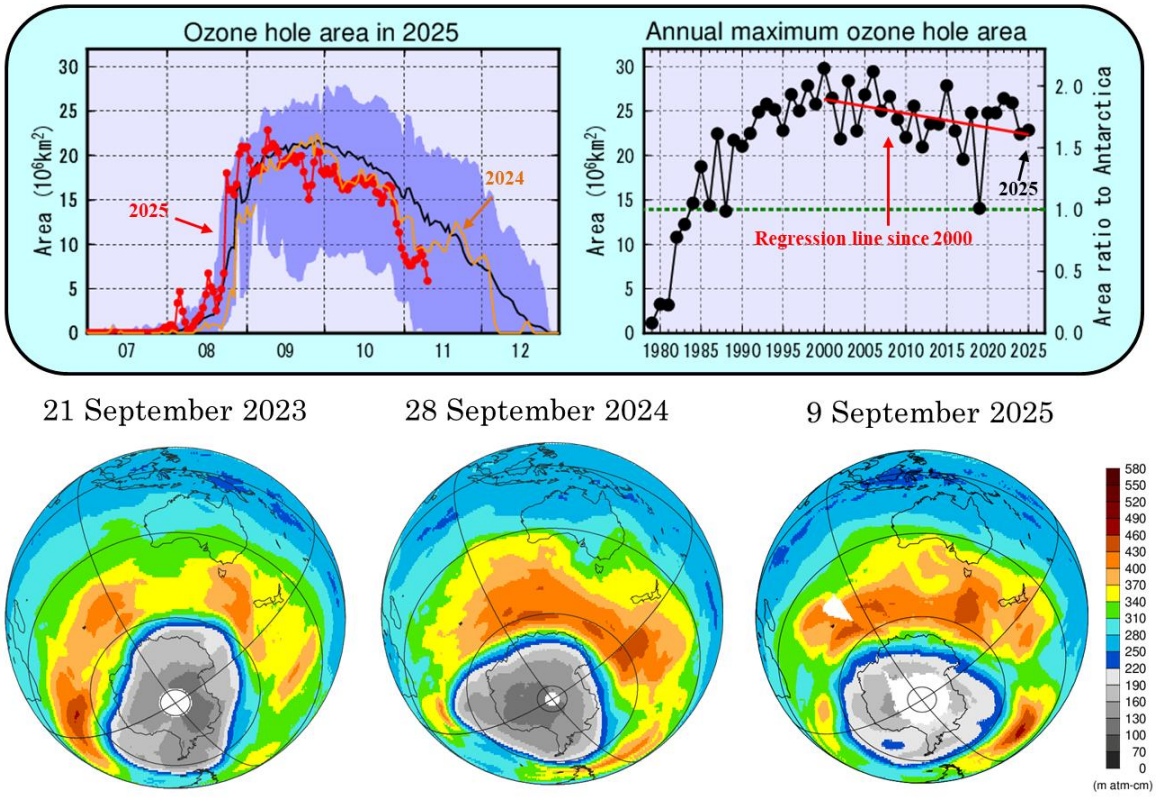

Figure 3-1 Antarctic ozone hole observation

Upper left: Time-series representation of the daily ozone hole area for 2025 (red line), 2024 (orange line) and the 2015 – 2024 average (black line). Blue shading represents the range of daily maxima and minima over the previous 10 years. JMA defines the extent of Antarctic ozone hole expansion area expanding as the area in which the total ozone column value is less than or equal to 220 m atm-cm.

Upper right: Inter-annual variability of the annual maximum ozone hole area. The green dotted line shows the area of the Antarctic Continent (13.9 million square kilometers).

Bottom: Snapshots of total column ozone distribution on the day of the annual maximum ozone hole area for the previous three years; the Antarctic ozone hole is shown in grey. Images are based on NASA satellite data.

(SUZUKI Takashi, Atmospheric Environment and Ocean Division)

<<Table of contents <Top of this article

Status of the Arctic Sea Ice in 2025

It is virtually certain that there has been a long-term decreasing trend of sea ice extent in the Arctic Ocean since 1979, when the current method of monitoring using satellite sensors began. The trend is statistically significant at a confidence level of 99%. The reduction in the annual minimum extent is particularly notable at 0.083 × 10^6 km^2 per year up to 2025 (Figure 4-1).

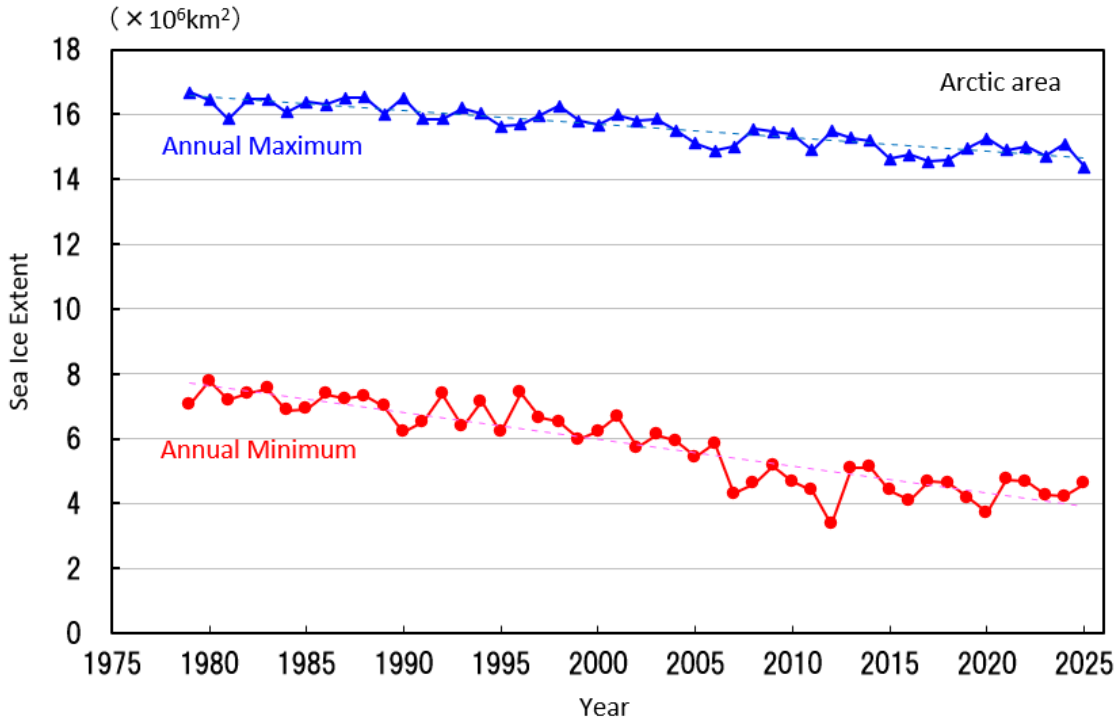

Figure 4-1 Time-series representations of annual maximum and annual minimum sea ice extent in the Arctic Ocean (including the Sea of Okhotsk and the Bering Sea) from 1979 to 2025

Blue and red lines indicate annual maximum and annual minimum sea ice extents, respectively, with dashed lines indicating linear trends. Sea ice extents are calculated from brightness temperature data provided by NASA (the National Aeronautics and Space Administration) and NSIDC (the National Snow and Ice Data Center).

Based on preliminary analysis, the annual maximum Arctic sea ice extent was 14.37 × 10^6 km^2 on 19 March 2025, marking the lowest value since 1979. The value subsequently decreased during spring and summer in the Northern Hemisphere and reached its annual minimum of 4.62 × 10^6 km^2 on 6 September, marking the 11th-lowest level since 1979 (Figures 4-2, 4-3).

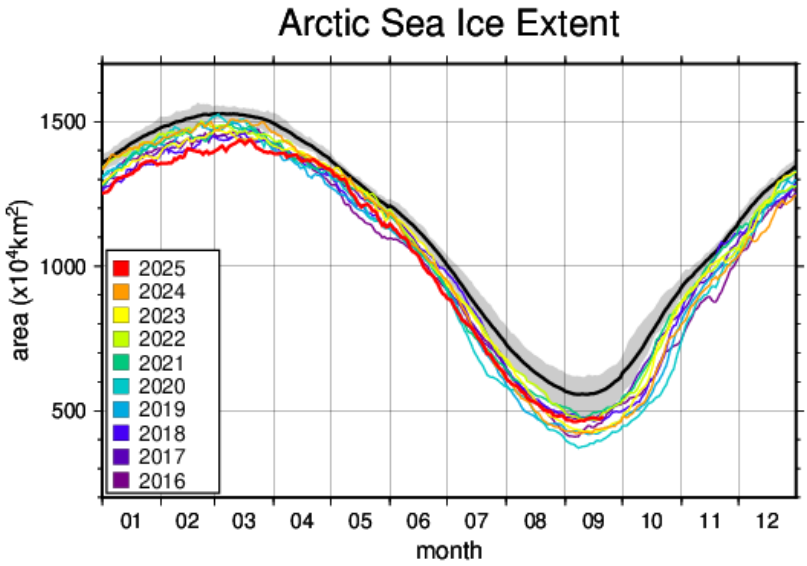

Figure 4-2 Annual variations in the Arctic sea ice extent

The black line represents the normal, and shading represents the normal range. The base period for the normal is 1991 – 2020.

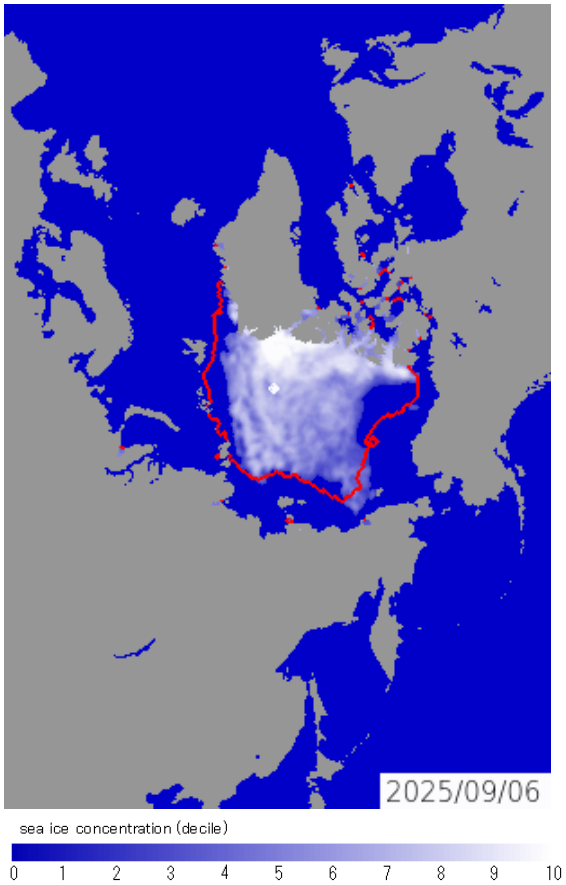

Figure 4-3 Annual minimum Arctic sea ice distribution

As of 6 September 2025. The red lines represent the normal extent. The base period for the normal is 1991 – 2020.

(HAMADA Keiji, Office of Marine Prediction)

<<Table of contents <Top of this article

Factors behind record-high temperatures over Japan in summer 2025 and dry conditions in July, and the large-scale atmospheric circulation behind heavy rainfall in the first half of August

In summer (June – August) 2025, Japan experienced sweltering heat with above-normal surface air temperatures in northern, eastern and western Japan, as well as notably high temperatures from mid-June to early August. In July, record-dry conditions were observed in parts of the country due to an inactive Baiu front and a suppressed supply of moisture. The nation's Hokuriku and Kyushu regions experienced heavy rainfall in the first half of August.

TCC issued a press release regarding the primary factors behind these anomalous climate conditions as summarized by the JMA Advisory Panel on Extreme Climatic Events (comprised of prominent climate science academics and researchers) on 5 September 2025.

The characteristics of the record-high temperatures seen in summer 2025 and the dry conditions observed in July in Japan can be summarized as follows (Figure 5-1):

- Summer mean temperatures far exceeding previous records set in 2023 and 2024.
- A new national record-high daily maximum temperature and unprecedented cumulative numbers of weather stations observing daily maximum temperatures exceeding certain thresholds
- Early seasonal march with the earliest-ever withdrawal of the Baiu rainy season over many regions, and consequent record-dry conditions over Hokuriku region in July

Factors behind these characteristics can be summarized as follows:

- Enhanced convection over the Asian monsoon region from the early summer monsoon period in association with above-normal ocean temperatures in the tropical western Pacific
  - ✓ This contributed to a markedly poleward-shifted subtropical jet over Eurasia from June onward and the Tibetan High extension toward Japan.
  - ✓ The North Pacific Subtropical High (NPSH) extended toward Japan in association with unprecedented intensification of cumulus convection to the east of the Philippines.
  - ✓ Both the Tibetan High and the NPSH covered areas around Japan, causing temperature rise under a dominant anomalous descent.
- A long-term tropospheric warming trend associated with global warming and pronounced above-normal tropospheric temperatures over the mid-latitude Northern Hemisphere in association with persistent remarkably high sea surface temperatures (SSTs) in the area in recent years

The large-scale atmospheric circulation behind the heavy rainfall observed in the first half of August and the effects of global warming in relation to these extreme events were also examined (see TCC press release).

The press release is available at https://www.data.jma.go.jp/tcc/data/news/press_20250930.pdf.

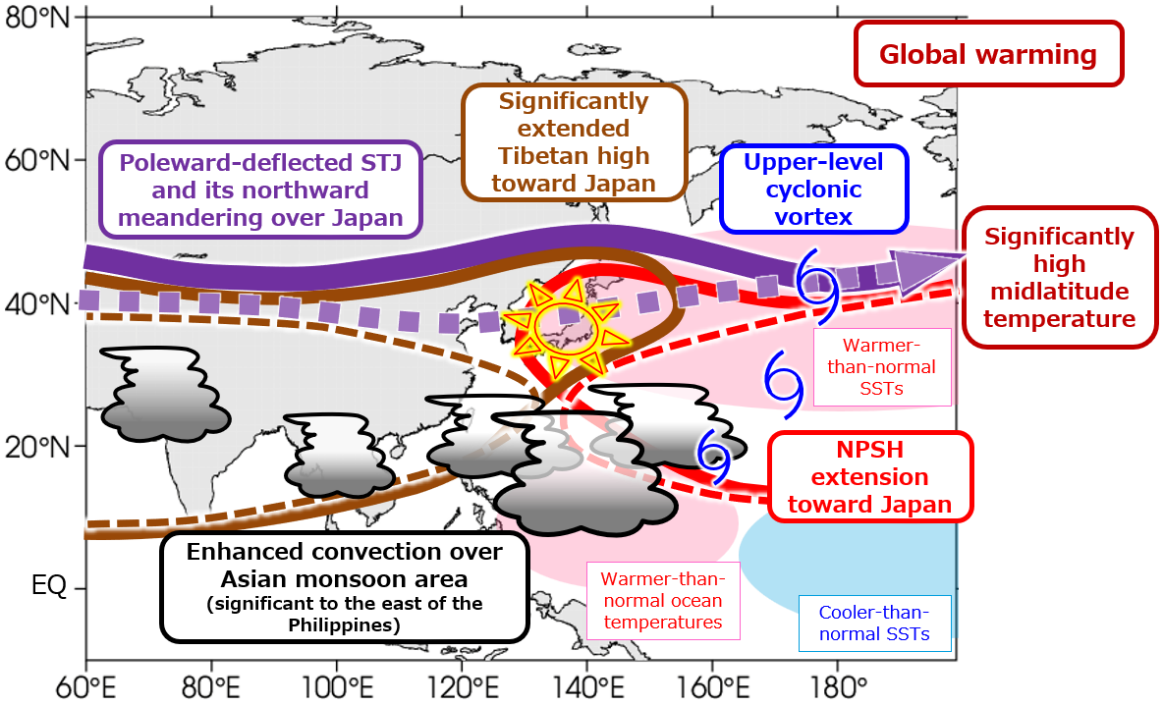

Figure 5-1 Large-scale factors behind record-high temperatures and dry conditions in summer 2025

"STJ," "SST" and "NPSH" stand for subtropical jet, sea surface temperature and North Pacific Subtropical High, respectively. Dashed lines show normal positions.

(TAKEMURA Kazuto, Tokyo Climate Center)

<<Table of contents <Top of this article

TCC and WMC Tokyo co-contributions to Regional Climate Outlook Forums in Asia

WMO Regional Climate Outlook Forums (RCOFs) bring together national, regional and international climate experts on an operational basis to produce regional climate outlooks based on inputs from participating NMHSs, regional institutions, Regional Climate Centres (RCCs) and global producers of climate predictions. By providing a platform for countries with similar climatological characteristics to discuss related matters, these forums ensure consistency in terms of access to and interpretation of climate information. In autumn 2025, representatives from TCC and the World Meteorological Centre (WMC) Tokyo attended two RCOFs in Asia:

- The 32nd session of the South Asian Climate Outlook Forum (SASCOF-32)
- The 25th session of the ASEAN Climate Outlook Forum (ASEANCOF-25)

1. SASCOF-32

The 32nd session of the South Asian Climate Outlook Forum (SASCOF-32) and Climate Services User Forum (CSUF) was hosted online by RCC-Pune on 25 September and 3 October 2025.

In Session II, titled "Seasonal Prediction of South Asia for OND Season 2025: Global and Regional Perspectives" on 25 September, a WMC Tokyo representative provided seasonal outlooks for October to December in South Asia based

on climate monitoring and forecast products from the TCC/WMC Tokyo website, consistent with Copernicus Climate Change Service (C3S) multi-model ensemble prediction incorporating JMA seasonal prediction. It was reported that La Niña-like conditions are likely to become clear toward early boreal winter together with negative Indian Ocean dipole-like conditions, but are not expected to persist.

2. ASEANCOF-25

The 25th session of the ASEAN Climate Outlook Forum (ASEANCOF-25) was hosted online by Cambodia's Ministry of Water Resources and Meteorology from 27 to 30 October 2025.

In a session titled "Regional Outlook (DJF 2025/2026) and Updates from Global Producing Centres/International Climate Centres" on 28 October, a WMC Tokyo representative provided winter outlooks for Southeast Asia based on climate monitoring and forecast products from the TCC/WMC Tokyo website, consistent with C3S multi-model ensemble prediction incorporating JMA seasonal prediction. Based on JMA's ensemble seasonal prediction system, above-normal precipitation is predicted in many parts of Southeast Asia due to La Niña-like conditions being likely to continue toward the first half of boreal winter. However, these conditions will rapidly weaken, making it likely that ENSO-neutral conditions will persist until late boreal winter.

These activities are intended to support the output of country-scale outlooks by National Meteorological and Hydrological Services (NMHSs), and to contribute to the summarization of consensus outlooks as well as the reduction of climate disaster risk in the water, agriculture and health sectors for each target area. TCC and WMC Tokyo are committed to ongoing collaboration with operational climate communities to enhance progress in forecast skill and application of climate information toward the resolution of common issues and the realization of a world resilient to adverse climate conditions.

(HARADA Masashi, KURAMOCHI Masaya [Tokyo Climate Center] and SATO Hitoshi [World Meteorological Centre Tokyo])

<<Table of contents <Top of this article

You can find the latest newsletter from the Japan International Cooperation Agency (JICA).
JICA Magazine
https://jicamagazine.jica.go.jp/en/
"JICA magazine" is a public relations magazine published by JICA. It introduces the current situations of developing countries around the world, the people who are active in the field, and the content of their activities.

Any comments or inquiry on this newsletter and/or the TCC website would be much appreciated.
Please e-mail to tcc@met.kishou.go.jp.
(Editors: HARADA Masashi, KURAMOCHI Masaya)

Tokyo Climate Center, Japan Meteorological Agency
3-6-9 Toranomon, Minato City, Tokyo 105-8431, Japan

TCC Website:
https://www.data.jma.go.jp/tcc/tcc/index.html